Enhanced Biosensor Based on Assembled Porous Silicon Microcavities Using CdSe/ZnS Quantum Dots

Miao Sun ⓘ, Shuangshuang Zhang ⓘ, Jiajia Wang, Zhenhong Jia ⓘ, Xiaoyi Lv ⓘ, and Xiaohui Huang ⓘ

Abstract—To further improve the sensitivity of porous silicon-assembled microcavity biosensors, the detection of porous silicon assembled microcavity by angle spectrum method is also researched. This contribution uses CdSe/ZnS quantum dot-labelled probe DNA to amplify the refractive index and detect it by the angle spectrum method. The first layer is a microcavity layer, and the next is porous silicon with a Bragg structure. After functionalization, different concentrations of target DNA were coupled to construct quantum dot-labelled probe DNA to bind specifically to the target DNA. With the Bragg device based on quartz glass forming an assembled microcavity structure, using a He-Ne laser as the detection light and collimation beam, the angle spectrum method is used to detect different concentrations of target DNA before and after biological reaction with quantum dot-labelled probe DNA and reflect the angle of minimum light intensity. The experimental results show that with increasing target DNA concentration, probe DNA concentration and angle, the detection limit is 13.25 pM. The angle-spectrum method has been successfully used to detect the assembled porous silicon microcavity. The angle-spectrum method has the advantages of spectrometer free and low cost.

Index Terms—Porous silicon, microcavity, angle spectrum, biosensor, quantum dots.

I. INTRODUCTION

POROUS silicon (PSi) has a large surface area, favourable biocompatibility, and adsorption and is widely used in biosensors. PSi has been widely used in the field of biosensors [1], [2] due to its large specific surface area, good biological compatibility and absorbability, and low fluorescence background after solution treatment, such as DNA [3], [4], antigens and antibodies [5], [6], enzymes [7], [8] and other sensitive elements. PSi can be prepared into a variety of biosensors with monolayer [9], [10], Bragg [11], [12], microcavity [13], [14] and other structures. Compared with the Bragg structure, the

Miao Sun and Shuangshuang Zhang are with the School of Physical Science and Technology, Xinjiang University, Urumqi 830046, China (e-mail: sunmiao0859@163.com; zhangshuangs1997@163.com).

Jiajia Wang, Zhenhong Jia, and Xiaohui Huang are with the School of Information Science and Engineering, Xinjiang University, Urumqi 830046, China, and also with the Key Laboratory of Signal Detection and Processing, Xinjiang Uygur Autonomous Region, Xinjiang University, Urumqi 830046, China (e-mail: wjjxj@xju.edu.cn; jzhh@xju.edu.cn; hxhdemail@sina.com).

Xiaoyi Lv is with the School of Software, Xinjiang University, Urumqi 830046, China, and also with the Key Laboratory of Signal Detection and Processing, Xinjiang Uygur Autonomous Region, Xinjiang University, Urumqi 830046, China (e-mail: xiaoz813@163.com).

Digital Object Identifier 10.1109/JPHOT.2021.3101656

microcavity (PSM) has the optical characteristics of half-height width and high transmittance at the resonance peak, so it has higher sensitivity [15]. Mariani et al. reported a label-free PSi interferometer that was 10000 times better than the direct (that is, non-amplified) label-free PSi biosensor and was able to specifically detect TNF-α at concentrations down to 3.0 nM, with a detection limit of 200 pM [16].

To solve the problem of the limitation of resolution in spectrometry, affecting the detection sensitivity of PSi biosensors, the angle spectrum method proposed by Li Peng et al. based on the relationship between the wavelength of peak resonance of PSM and the angle of incident light has been used to measure the change in angle of PSM devices before and after biological reactions [17].

Quantum dots (QDs) have the advantages of high photoelectric conversion efficiency, long fluorescence lifetime, controllable surface characteristics, etc. [18]. The modified group on the surface of the modified group can be covalently connected with the group on the biomolecule, which has good biological compatibility. According to the different characteristics of QDs, high-sensitivity biological detection can be realized [19], [20]. The detection mechanism of biomolecules labelled by QDs mainly includes detecting biomolecules or probe molecules labelled by QDs [2], [21] and realizing refractive index amplification by using a high refractive index of QDs [22]. Biomolecules or probe molecules are detected by QDs labelling, photoluminescence is performed under excitation light, and biological detection is achieved by detecting fluorescence intensity [23], [24]. Biomolecules or probe molecules are detected by QDs labelling, and the high refractive index of QDs is used to achieve refractive index amplification, measure the change in refractive index before and after biological reaction, and detect the change in reflection spectrum or angle spectrum caused by it to achieve biological detection [22]. Wei Hanyue et al. proposed a new low-cost biological detection method based on the digital imaging of PSi surface fluorescence, which enhanced the fluorescence generated by QDs through a Bragg mirror, obtained a fluorescence image of the PSi surface through a digital microscope, and detected the target DNA by calculating the average grey value of the image to obtain a detection limit of 88 pM [23]. In this paper, QDs were used to label probe DNA, and the high refractive index of QDs was used to achieve highly sensitive biological detection.

To solve the problem that biomolecules enter to finite depths [25], [26]. PSi photonic crystals have not been fully utilized, so there is a large difference between theoretical and experimental
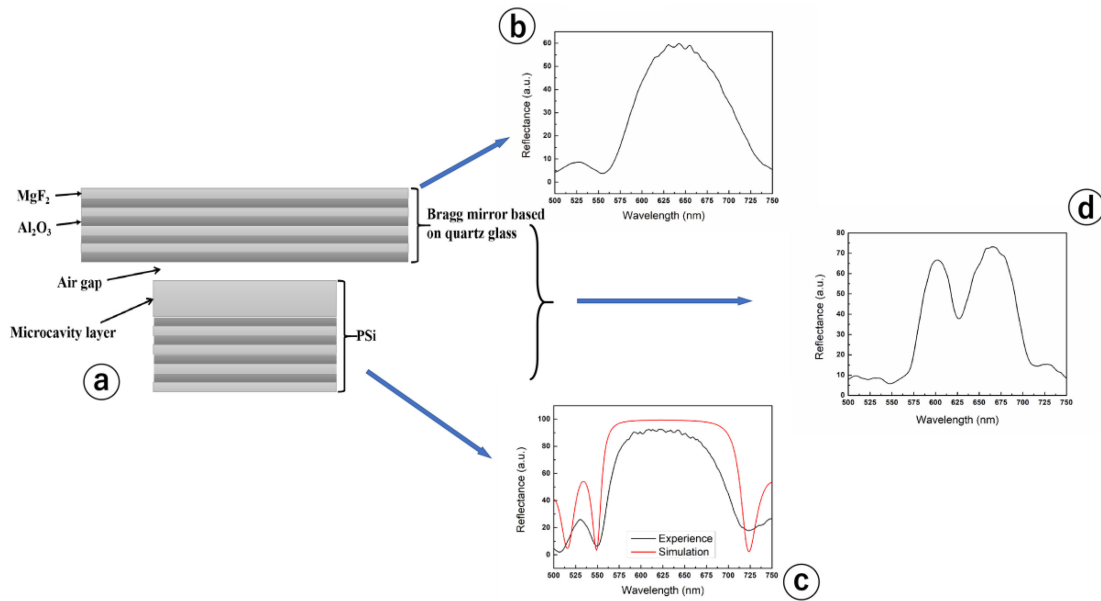
Fig. 1. Structure diagram of assembled microcavity. (a) Structure diagram of assembled microcavity; (b) Reflection spectra of a Bragg mirror based on quartz glass; (c) Reflection spectra of Porous silicon; d: Reflection spectra of assembled microcavity obtained after assembly.

detection sensitivity; our team designed an assembled microcavity [27], in which biomolecules can directly enter the defect layer of porous silicon, thus improving the sensitivity of porous silicon optical biosensor. This paper based on porous silicon assembled microcavity, the probe DNA of different concentrations was labeled by QDs to amplify the refractive index, and the angle spectrum detection method was used for detection to obtain a lower detection limit. The advantages of this paper are as follows: 1) Using the high refractive index of QDs, the probe molecule is amplified to improve the sensitivity of the biosensor; 2) Due to the limited detection methods that can be used to assemble the microcavity, we studied the angle spectrum method for its detection, using a detector to receive the reflected light, calculate the change of the angle before and after the biological reaction, and get a lower detection limit. The advantages of this method are spectrometer free and low cost.

II. THEORETICAL ANALYSIS

A. Theory of Assembled Microcavities

In previous research, we designed an assembled microcavity [28], as shown in Fig. 1(a), the microcavity is designed as two separate parts, on half PSi Bragg mirror to quartz substrate Bragg reflector instead of (traced purchased from Shanghai industrial development co., LTD.), It is alternately composed of MgF_2 and Al_2O_3 thin films, a total of 6 cycles, 12 layers. The refractive index of MgF_2 and Al_2O_3 is 1.37 and 1.58, respectively, and the thickness is 115.51 nm and 100.16 nm, respectively. The central wavelength measured by a reflection spectrometer (Hitachi U-4100, purchased from Hitachi, Japan) is 633 nm. The reflection spectrum is shown in Fig. 1(b). The lower part is made of porous silicon and consists of a microcavity in the first layer and a Bragg mirror in the following. Its central wavelength is designed at 650 nm, as shown in Fig. 1(c).
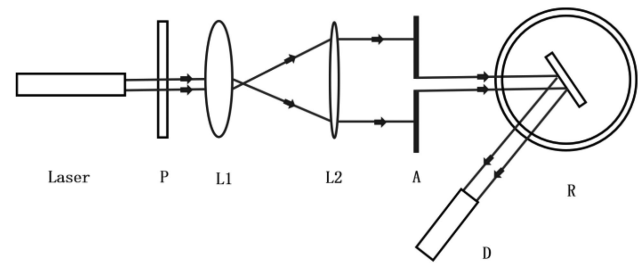

Fig. 2. Schematic diagram of the experimental setup of the angle spectrum method.

B. Detection Method

After assembly, the angle spectrum method is used for detection. Biomolecules enter the PSi layer, causing the effective refractive index to increase in each layer, and the wavelength of the resonance peak λ redshifts, but with increasing incident angle, the wavelength of the resonance peak blueshifts. The principle diagram of the experimental device is shown in Fig 2. An incident laser (He-Ne laser) with a single wavelength of λ_i is used as the incident light source. After the beam is collimated and expanded, it reaches the surface of the assembled microcavity, which receives the reflected light with a detector. When biological molecules are added to the PSi devices, each layer of the refractive index increases, and the resonance peak wavelength increases. Biological detection is performed, in which the angle of incidence is adjusted to θ_1, the light intensity is adjusted, and the lowest layer of the PSi microcavity in the biological reaction is added after the refractive index is increased again. The incident light is adjusted to θ_2 to achieve the minimum value. Again, according to the angle change $\Delta\theta = \theta_2 - \theta_1$, the refractive index Δn changes [24].
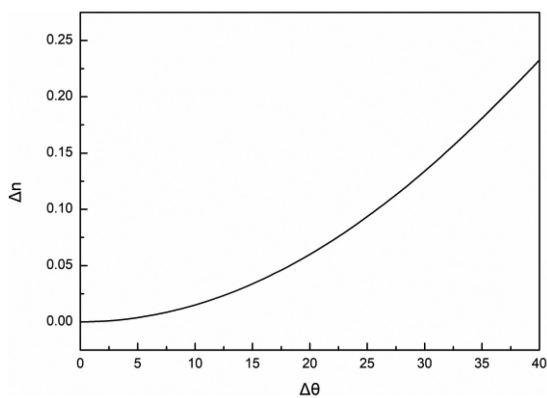
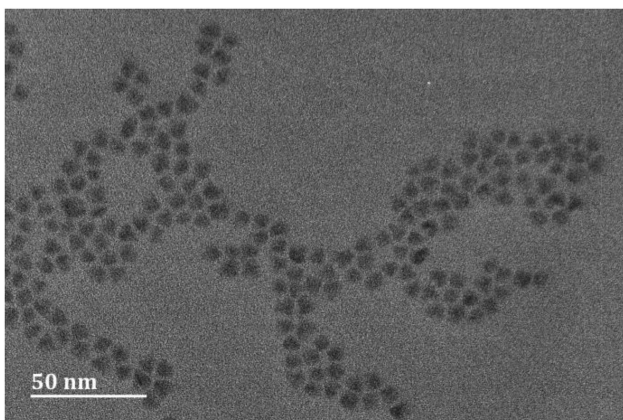Fig. 3. Relationship between different Angle and refraction changes.

Fig. 4. High-resolution transmission electron microscopy image of QDs.

Through the theoretical simulation of the transfer matrix method, the relationship between the change of incident Angle $\Delta\theta$ and the change of refractive index Δn is obtained, as shown in Fig. 3. It can be seen from the figure that the smaller the slope is, the higher the sensitivity of the device is, so the detection is more favorable when the incident Angle is small. Therefore, when designing the device, the central wavelength is close to 633 nm.

III. EXPERIMENTAL SECTION

In the experiment, the anodic electrochemical corrosion method was used prepare of porous silicon [27]–[29]. The first layer is a microcavity. The Bragg structure is shown below. To conjugate biomolecules, we must functionalize PSi, including three processes: oxidation, silanization and glutaraldehyde treatment [22], [30], [31]. The functionalized porous silicon has a large number of aldehyde groups on its surface, which can be connected with the modified amino group on the target biomolecule to make it fixed in the porous silicon. The reaction process is shown in Fig. 6 (2, 3, 4).

A. The Target DNA is Fixed on the Porous Silicon Wall

The target DNA (5'-GTTGCAACGTCACATG-3'-NH$_2$, 16 base pairs), and the length of the DNA strand was approximately
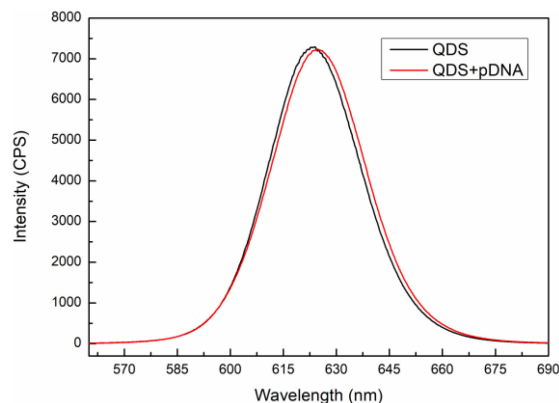

Fig. 5. QD fluorescence spectrograms before and after coupling with probe DNA.

5.44 nm. With trace moving liquid concentrations of 0.2 nM, 0.1 nM, 0.05 Nm, 0.02 nM. Target DNA (40 μL) was dropped onto the surface of PSi devices in a constant temperature box at 37 °C for approximately 2 h, and the target DNA on the amino(-NH$_2$) and aldehyde groups(-CHO) fully reacted in the PSi. Phosphate buffer and deionized water were flushed repeatedly to remove unreacted target DNA and dried in an air environment. Then, the PSi microcavity sample was immersed in 3 M ethanolamine hydrochloride solution and placed in an incubator at 37 °C for approximately 1 h. The unreacted aldehyde group was sealed. After removal, the sample was rinsed repeatedly with phosphate buffer solution and deionized water and then dried in air. Fig. 6(5) shows its reaction process.

B. QDs Labelled Probe DNA

Carboxyl water-soluble CdSe/ZnS QDs (purchased from Wuhan Jiayuan Quantum Dot Co., Ltd., China) have a CdSe core structure with an internal structure surrounded by a ZnS shell and a surface modified with a carboxyl group (- COOH). The emission peak is 625 nm, and the average particle size is 9 nm, as shown in Fig. 4. Thirty microlitres of QDs-COOH (8 μM) was taken, and 200 μL of PBS was added. Then, 20 μL of EDC (0.01 M) and NHS (0.01 M) were added to activate the carboxyl group. The reaction time was 30 min at room temperature, and the concentration of QDs-COOH after dilution was 1 μM. Two hundred microlitres of probe DNA (5'-CAACGTTGCAGTGTAC-3'-NH$_2$, 16 base pairs) with a concentration of 10 μm was added to the diluted QDs-COOH solution, which was shaded from light for 10 h to ensure that the carboxyl group on QDs-COOH was fully connected with the amino group on probe DNA and then centrifuged in a 10000 r/min centrifuge for 15 min to leave precipitates in the supernatant.

To prove that QDs-COOH was successfully linked to probe DNA, the fluorescence peak of QDs-COOH before and after coupling with probe DNA was detected by a Hitachi F4600 fluorescent spectrometer (purchased from Hitachi, Japan, with wavelength resolution of 0.2 nm). The excitation wavelength was 375 nm, the excitation voltage was 700 V, and the seam
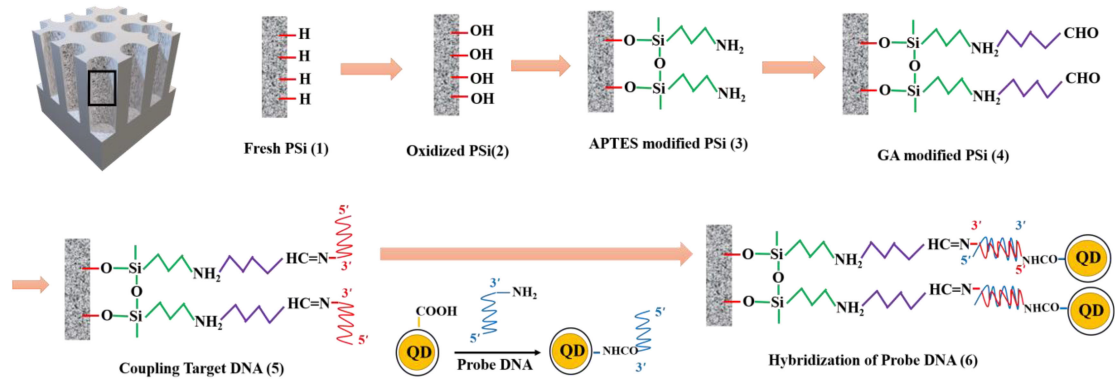
Fig. 6.   Modification of porous silicon and occurrence of biological reactions.

width was 10 nm. The results showed that the fluorescence peak of QDs-COOH without probe DNA coupling was at 623 nm. After coupling with probe DNA at a concentration of 10 μm, as the quantum dots grow in size, the fluorescence peak position changed to 626 nm, and the redshift was 3 nm [23], indicating that the QDs were successfully coupled with probe DNA, as shown in Fig. 5.

C. Target DNA was Hybridized With QD-pDNA

A pipettor was used to hybridize QDs-pDNA onto half the surface of a PSi device where the target DNA had been fixed. The other half was used as the control area, without adding QDs-pDNA, and stood for 2 h in a 37°C thermostatic chamber. After removal, the QDs-pDNA was rinsed repeatedly with PBS and deionized water and dried in air to remove the QDs-pDNA that was not connected successfully and the QDs-pDNA that failed to enter the hole for the hybridization reaction. The preparation process is shown in Fig. 6(6).

IV.   Results and Discussion

A. Assembly and Detection of Assembled Microcavity

The fabricated quartz glass-based Bragg mirrors were fitted together with PSi, and the size and uniformity of the air slits were controlled by custom clamps. Because we used half the region plus QDs-pDNA for biological reaction, forming the reaction region, the other half did not react without QDs-pDNA, forming a control area. Therefore, the thickness of the air slits in the two regions after assembly was the same, which corresponded to two identical PSi microcavities, including the microcavity in the control region before biological reaction and the microcavity in the reaction region after the biological reaction. After the successful fabrication of the assembled microcavity, the position of the resonant peak was different due to the change in the central wavelength of PSi and the thickness of the air slit, leading to the inconsistency between the central wavelength of the resonant peak and the wavelength of the incident light. The oblique incident method could make the central wavelength of the assembled microcavity device consistent with the incident light source. If the incident light did not cross the area at first to control the reaction, with reflected light intensity of the

minimum angle $\theta 1$, then the incident light aimed to join half the area of the QD-labelled probe DNA. The reflected light intensity of the minimum angle θ_2 changed the angle of the hybridization reaction before and after $\Delta\theta = \theta_2$-θ_1. To accurately find the position of the minimum light intensity, the light intensity with every 1' change in angle was recorded near the position of the minimum light intensity, and the result is shown in Fig. 7.

The change in angle before and after adding the QD-labelled probe DNA was 3.11°, which proves that the target DNA and probe underwent a hybridization reaction, increasing the effective refractive index of the assembled microcavity device. The redshift of the angle spectrum is shown.

B. Verification of Whether There are Residual Quantum Dots in Porous Silicon

A Hitachi F4600 fluorescent spectrometer (purchased from Hitachi, Japan, with wavelength resolution of 0.1 nm) was used to detect whether the QDs that had been cleaned were present in the holes of the PSi device. The residual QDs in PSi were because, on the one hand, the QDs were not successfully coupled to the probe DNA. On the other hand, the QDs were successfully coupled to the probe DNA but failed to hybridize with the target DNA. Because PSi is functionalized and its surface groups are closed, QDs cannot be directly connected to the pore wall of PSi. As shown in Fig. 8, the excitation wavelength was 375 nm, the excitation voltage was 700 V, and the seam width was 5 nm. The black curve indicates that the QDs directly dripped onto the functionalized PSi, while the red curve indicates that the QDs were labelled with probe DNA and then coupled to the functionalized PSi. The results indicate that if the QDs cannot connect to the probe DNA successfully, the QDs will not enter the PSi holes.

C. Measurement Results and Discussion of the Angle Spectrum Method

Target DNA at concentrations of 0.2 nM, 0.1 nM, 0.05 nM and 0.02 nM was fixed in PSi and hybridized with probe DNA labelled with QDs. The redshifts with angle spectrum test-detected angles $\Delta\theta$ were 3.11°, 1.28°, 0.78° and 0.39°, and the results of fitting are shown in Fig. 9. The linear equation was Y = 15.17X
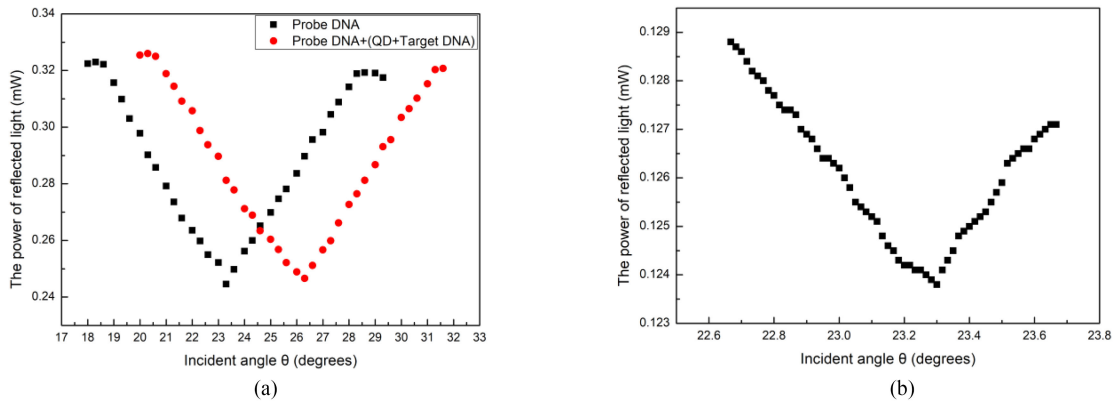
Fig. 7. (a) Angle spectrum before and after the hybridization reaction. The black curve represents the angle spectrum of the control region before the hybridization reaction, and the red curve represents the angle spectrum of the DNA region coupled with the QD-labelled probe. (b) Angle spectrum in the range of 1' at the minimum light intensity.
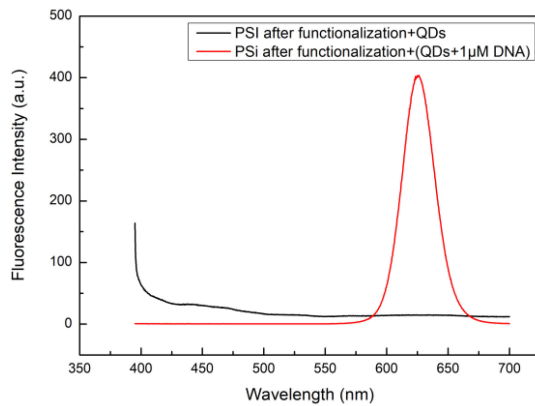

Fig. 8. The red curve represents the fluorescence spectrum of the functionalized porous silicon device with quantum dot-labelled 1 nM probe DNA, and the black curve represents the fluorescence spectrum of the functionalized porous silicon device after the addition of quantum dots.
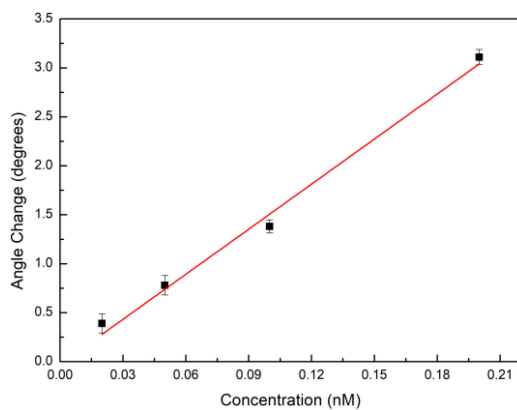

Fig. 9. Relationship between target DNA and angular spectral redshift at different concentrations.

$+0.012$, where X represents the target DNA concentration (nM), Y is the amount of redshift $\Delta\theta$ before and after hybridization, the slope is 15.17, and the linear correlation coefficient $R^2 = 0.99$.

Because the surface of the PSi device features undulation, it will cause random error in measurements. In the experiment, the 3σ rule was used to calculate the experimental results. Using the same PSi blank sample, the position of the minimum reflected light intensity was measured continuously 10 times, and the standard deviation σ was obtained by Equation.

$$\sigma = \sqrt{\frac{\sum_{i=1}^{n}\left(X_i - \overline{X}\right)^2}{n-1}} \tag{1}$$

where σ represents the standard deviation of the minimum position of the reflected light intensity for 10 consecutive measurements, n represents the number of measurements, and X represents the position of the minimum value of the reflected light intensity. The σ obtained by the experiment was 0.067. Taking the probe DNA concentration corresponding to the angle change of 3σ as the detection limit, the detection limit can be obtained as 13.25 pM according to the linear equation.

In previous reports, Zhou Rui et al. used CdSe/ZnS QDs to label target DNA and magnify the refractive index of reactants based on PSi microcavity devices. The hybridization reaction between probe DNA and target DNA labelled with QDS at different concentrations was detected by the angle spectrum detection method of free spectrum equipment, and a detection limit of 35.9 pM was obtained. Compared with the experimental results reported above, our proposed assembled microcavity features a lower detection limit [15].

V. CONCLUSION

In this paper, CdSe/ZnS water-soluble QDs was used as the marker to successfully label 16 base pairs of probe DNA, and the high refractive index of the reactants was amplified by the high refractive index of quantum dots. In addition, the detection of porous silicon assembled microcavity by Angle spectrum method was studied. A new PSi assembly microcavity device was proposed, which could enable biomolecules to enter the microcavity layer directly, thus improving the sensitivity of PSi. The first layer of the microcavity was etched, and PSi with a six-period Bragg structure was functionalized. The probe DNA labelled with QDs was added to half the surface of the PSi

with target DNA fixed, and the hybridization reaction took place there, while the other half did not undergo biological reaction and was used as a control experiment. The prepared PSi was assembled with a quartz-based Bragg mirror and measured by the angle spectrum method. According to the measurement results, the redshift of the resonance peak angle before and after the biological reaction was linearly related to the concentration of the target DNA, and the detection limit was estimated to be 13.25 pM by curve fitting. The advantages of Angle spectrum method are spectrometer free, low cost, and high detection sensitivity.

REFERENCES

[1] N. Abu-Thabit and E. Ratemi, "Hybrid porous silicon biosensors using plasmonic and fluorescent nanomaterials: A mini review," *Front. Chem. Rev.*, vol. 8, no. 7, May 2020, Art. no. 454, doi: 10.3389/fchem.2020.00454.

[2] S. Arshavsky-Graham, N. Massad-Ivanir, E. Segal, and S. Weiss, "Porous silicon-based photonic biosensors: Current status and emerging applications," *Anal. Chem.*, vol. 91, no. 1, pp. 441–467, Jan. 2019, doi: 10.1021/acs.analchem.8b05028.

[3] Y. Zhao, J. L. Lawrie, K. R. Beavers, P. E. Laibinis, and S. M. Weiss, "Effect of DNA-induced corrosion on passivated porous silicon biosensors," *ACS Appl. Mater. Interf.*, vol. 6, no. 16, pp. 13510–13519, 2014, doi: 10.1021/am502582s.

[4] R. Vilensky, M. Bercovici, and E. Segal, "Oxidized porous silicon nanostructures enabling electrokinetic transport for enhanced DNA detection," *Adv. Funct. Mater.*, vol. 25, no. 43, pp. 6725–6732, 2015, doi: 10.1002/adfm.201502859.

[5] C. Rodriguez *et al.*, "Gold nanoparticle triggered dual optoplasmonic-impedimetric sensing of prostate-specific antigen on interdigitated porous silicon platforms," *Sens. Actuat. B: Chem.*, vol. 267, pp. 559–564, doi: 10.1016/j.snb.2018.03.179.

[6] E. Mauriz, M. C. García-Fernández, and L. M. Lechuga, "Towards the design of universal immunosurfaces for SPR-based assays: A review," *TrAC Trends Anal. Chem.*, vol. 79, pp. 191–198, 2016, doi: 10.1016/j.trac.2016.02.006.

[7] S. N. Jenie, B. Prieto-Simon, and N. H. Voelcker, "Development of L-lactate dehydrogenase biosensor based on porous silicon resonant microcavities as fluorescence enhancers," *Biosens. Bioelectron.*, vol. 74, pp. 637–643, Dec. 2015, doi: 10.1016/j.bios.2015.07.025.

[8] S. Mariani, L. M. Strambini, and G. Barillaro, "Femtomole detection of proteins using a label-free nanostructured porous silicon interferometer for perspective ultrasensitive biosensing," *Anal. Chem.*, vol. 88, no. 17, pp. 8502–8509, Sep. 2016, doi: 10.1021/acs.analchem.6b01228.

[9] S. Mariani *et al.*, "Moldless printing of silicone lenses with embedded nanostructured optical filters," *Adv. Funct. Mater.*, vol. 30, no. 4, Jan. 23 2020, Art. no. 1906836, doi: 10.1002/adfm.201906836.

[10] S. Mariani *et al.*, "Layer-by-layer biofunctionalization of nanostructured porous silicon for high-sensitivity and high-selectivity label-free affinity biosensing," *Nature Commun.*, vol. 9, no. 1, Dec. 10 2018, Art. no. 5256, doi: 10.1038/s41467-018-07723-8.

[11] D. Kou, S. Zhang, J. L. Lutkenhaus, L. Wang, B. Tang, and W. Ma, "Porous organic/inorganic hybrid one-dimensional photonic crystals for rapid visual detection of organic solvents," *J. Mater. Chem. C*, vol. 6, no. 11, pp. 2704–2711, 2018, doi: 10.1039/c7tc05390h.

[12] N. Massad-Ivanir, S. K. Bhunia, R. Jelinek, and E. Segal, "Porous silicon bragg reflector/carbon dot hybrids: Synthesis, nanostructure, and optical properties," *Front Chem.*, vol. 6, 2018, Art. no. 574, doi: 10.3389/fchem.2018.00574.

[13] S. Surdo and G. Barillaro, "Impact of fabrication and bioassay surface roughness on the performance of label-free resonant biosensors based on one-dimensional photonic crystal microcavities," *ACS Sens.*, vol. 5, no. 9, pp. 2894–2902, Sep. 25, 2020, doi: 10.1021/acssensors.0c01183.

[14] S. N. A. Jenie, S. Pace, B. Sciacca, R. D. Brooks, S. E. Plush, and N. H. Voelcker, "Lanthanide luminescence enhancements in porous silicon resonant microcavities," *ACS Appl. Mater. Interf.*, vol. 6, no. 15, pp. 12012–12021, 2014, doi: 10.1021/am500983r.

[15] W.-T. Tsai, M.-H. Nguyen, J.-R. Lai, H.-B. Nguyen, M.-C. Lee, and F.-G. Tseng, "ppb-level heavy metal ion detection by electrochemistry-assisted nanoPorous silicon (ECA-NPS) photonic sensors," *Sens. Actuat. B: Chem.*, vol. 265, pp. 75–83, 2018, doi: 10.1016/j.snb.2018.01.232.

[16] S. Mariani, L. Pino, L. M. Strambini, L. Tedeschi, and G. Barillaro, "10 000-fold improvement in protein detection using nanostructured porous silicon interferometric aptasensors," *ACS Sens.*, vol. 1, no. 12, pp. 1471–1479, 2016, doi: 10.1021/acssensors.6b00634.

[17] P. Li *et al.*, "Spectrometer-free biological detection method using porous silicon microcavity devices," *Opt. Exp.*, vol. 23, no. 19, pp. 24626–24633, Sep. 2015, doi: 10.1364/oe.23.024626.

[18] J. Shu and D. Tang, "Current advances in quantum-dots-based photoelectrochemical immunoassays," *Chem. Asian J.*, vol. 12, no. 21, pp. 2780–2789, Nov. 2017, doi: 10.1002/asia.201701229.

[19] Z. Qiu *et al.*, "CdTe/CdSe quantum dot-based fluorescent aptasensor with hemin/G-quadruplex DNzyme for sensitive detection of lysozyme using rolling circle amplification and strand hybridization," *Biosens. Bioelectron.*, vol. 87, pp. 18–24, Jan. 2017, doi: 10.1016/j.bios.2016.08.003..

[20] Z. Qiu, J. Shu, and D. Tang, "Bioresponsive release system for visual fluorescence detection of carcinoembryonic antigen from mesoporous silica nanocontainers mediated optical color on quantum dot-enzyme-impregnated paper," *Anal. Chem.*, vol. 89, no. 9, pp. 5152–5160, May 2017, doi: 10.1021/acs.analchem.7b00989.

[21] D. Dovzhenko *et al.*, "Enhancement of spontaneous emission of semiconductor quantum dots inside one-dimensional porous silicon photonic crystals," *Opt Exp.*, vol. 28, no. 15, pp. 22705–22717, Jul. 2020, doi: 10.1364/OE.401197.

[22] R. Zhou, Z. H. Jia, X. Y. Lv, and X. H. Huang, "The enhanced sensitivity of a porous silicon microcavity biosensor based on an angular spectrum using CdSe/ZnS quantum dots," *Sensors*, vol. 19, no. 22, Nov. 2019, Art. no. 4872, doi: 10.3390/s19224872.

[23] H. Y. Wei *et al.*, "Detection using a quantum dots/porous silicon optical biosensor based on digital fluorescence images," *Sens. Actuat. B-Chem.*, vol. 315, no. 8, Jul. 2020, Art no. 128108, doi: 10.1016/j.snb.2020.128108.

[24] Y. Lin, Q. Zhou, D. Tang, R. Niessner, H. Yang, and D. Knopp, "Silver nanolabels-assisted ion-exchange reaction with cdte quantum dots mediated exciton trapping for signal-on photoelectrochemical immunoassay of mycotoxins," *Anal. Chem.*, vol. 88, no. 15, pp. 7858–7866, Aug. 2016, doi: 10.1021/acs.analchem.6b02124.

[25] D. Gerace *et al.*, "Modulation of quantum dot photoluminescence in porous silicon photonic crystals as a function of the depth of their penetration," in *Proc. Spie Photon. Europe*, 2016, Art. no. 988507.

[26] L. M. Karlsson, R. Tengvall, I. Lundstrom, and H. Arwin, "Penetration and loading of human serum albumin in porous silicon layers with different pore sizes and thicknesses," *J. Colloid Interface Sci.*, vol. 266, no. 1, pp. 40–47, Oct. 2003, doi: 10.1016/s0021-9797(03)00595-2.

[27] M. Sun, S. Zhang, Z. Jia, X. Lv, and X. Huang, "A biosensor based on an assembled porous silicon microcavity," *IEEE Sensors J.*, vol. 21, no. 9, pp. 10563–10570, 2021.

[28] Z. Y. Liu *et al.*, "Research on micro-cavity structure processing technology based on porous silicon," *Modern Phys. Lett. B*, vol. 34, no. 29, 2020, Art. no. 2050319, doi: 10.1142/s0217984920503194.

[29] S. Zhang, M. Sun, J. Yang, Z. Jia, X. Lv, and X. Huang, "Research on biological detection based on reflected light images of a porous silicon Bragg mirror," *IEEE Photon. J.*, vol. 13, no. 2, Apr. 2021, Art. no. 6800113.

[30] Y. Zhao, G. Gaur, S. T. Retterer, P. E. Laibinis, and S. M. Weiss, "Flow-through porous silicon membranes for real-time label-free biosensing," *Anal. Chem.*, vol. 88, no. 22, pp. 10940–10948, 2016, doi: 10.1021/acs.analchem.6b02521.

[31] V. Robbiano *et al.*, "Room-temperature low-threshold lasing from monolithically integrated nanostructured porous silicon hybrid microcavities," *ACS Nano*, vol. 12, no. 5, pp. 4536–4544, 2018, doi: 10.1021/acsnano.8b00875.